

Temperature effects on nuclear pseudospin symmetry in the Dirac-Hartree-Bogoliubov formalism

R. Lisboa

*Universidade Federal do Rio Grande do Norte,
Escola de Ciências e Tecnologia,
59078-970 Natal, Rio Grande do Norte, Brazil**

P. Alberto

*CFisUC, University of Coimbra, Physics Department,
P-3004-516 Coimbra, Portugal*

B. V. Carlson and M. Malheiro

*Departamento de Física,
Instituto Tecnológico da Aeronáutica,
Centro Técnico Aeroespacial,
12228-900 São José dos Campos,
São Paulo, Brazil*

(Dated: September 1, 2017)

Abstract

We present finite temperature Dirac-Hartree-Bogoliubov (FTDHB) calculations for the tin isotope chain to study the dependence of pseudospin on the nuclear temperature. In the FTDHB calculation, the density dependence of the self-consistent relativistic mean fields, the pairing, and the vapor phase that takes into account the unbound nucleon states are considered self-consistently. The mean field potentials obtained in the FTDHB calculations are fit by Woods-Saxon (WS) potentials to examine how the WS parameters are related to the energy splitting of the pseudospin pairs as the temperature increases. We find that the nuclear potential surface diffuseness is the main driver for the pseudospin splittings and that it increases as the temperature grows. We conclude that pseudospin symmetry is better realized when the nuclear temperature increases. The results confirm the findings of previous works using RMF theory at $T = 0$, namely that the correlation between the pseudospin splitting and the parameters of the Woods-Saxon potentials implies that pseudospin symmetry is a dynamical symmetry in nuclei. We show that the dynamical nature of the pseudospin symmetry remains when the temperature is considered in a realistic calculation of the tin isotopes, such as that of the Dirac-Hartree-Bogoliubov formalism.

PACS numbers: 21.10.-k, 21.60.CS, 21.60.Jz, 25.70.Mn

* ronai@ect.ufrn.br

I. INTRODUCTION

Since the seminal article published by Ginocchio 20 years ago [1], pseudospin symmetry has been extensively studied in RMF and Hartree-Fock theories, with the intention of understanding the origin of pseudospin symmetry and its symmetry-breaking.

The evidence for pseudospin symmetry comes from nuclear energy spectra with quasi degeneracy between pairs of single-particle states with quantum numbers $(n, l, j = l + 1/2)$ and $(n - 1, l + 2, j = l + 3/2)$ in a spherical basis where, n , l , and j are the radial, the orbital, and the total angular momentum quantum numbers, respectively, of the upper component of the Dirac spinor. Pseudospin symmetry was recognized as a relativistic symmetry when Ginocchio point out the pseudospin doublets can be written as $(\tilde{n} = n - 1, \tilde{l} = l + 1, \tilde{j} = \tilde{l} \pm 1/2)$ where, the quantum numbers \tilde{n} , \tilde{l} , and \tilde{j} are the quantum numbers of the lower component of the Dirac spinor [1, 2]. Pseudospin symmetry is exact when the doublets with $j = \tilde{l} \pm \tilde{s}$ are degenerate.

In RMF theory the Dirac equation with attractive scalar, $-V_S(r)$, and repulsive vector, $V_V(r)$, potentials displays exact pseudospin symmetry when $\Sigma(r) = V_S(r) + V_V(r) = 0$ or more generally, when $\Sigma'(r) = d\Sigma(r)/dr = 0$ [3, 4]. Since $\Sigma(r)$ plays the role of the nuclear binding potential, bound states cannot exist for $\Sigma(r) = 0$. In fact, for realistic nuclei, the cancellation between scalar and vector potentials gives a relatively small binding potential of about -60 MeV at the center. Thus pseudospin symmetry cannot be exact. The purpose the studies performed in most works on pseudospin symmetry is to understand its origin and its symmetry-breaking [5, 6].

The Dirac equation has been solved for different potentials and systems to study how the pseudospin doublets become degenerate or almost degenerate. Usually, the pseudospin splitting depends on the shape of the potentials that are used to solve the Dirac equation. In previous works [7, 8], the Woods-Saxon potential was used because the conditions $\Sigma(r) = 0$ and $\Sigma'(r) = 0$ can be met approximately by varying the parameters of this potential. The pseudospin splitting depends on the depth of $|\Sigma_0|$, its surface diffuseness and its radius. Then, the authors reduced the Dirac equation into two Schrödinger-like equations for the lower (and upper) spinor component, each being a sum of different terms: kinetic, pseudospin-orbit (and spin-), a Darwin term, and potential terms with $\Sigma(r)$ and $\Delta(r)$ potentials. By taking the expectation values of these terms, one obtains an energy decomposition

for each single-particle level, allowing the study of the non-perturbative nature of pseudospin symmetry. The pseudospin-orbit term has the denominator $E - \Sigma(r)$ and thus becomes infinite when $E = \Sigma(r)$, but the singularity is canceled by kinetic and Σ terms originating in the quasi-degeneracy [8]. In fact, a cancellation exists between the large pseudospin-orbit potential and other terms, showing the dynamic character of the pseudospin symmetry and its non-perturbative nature [5–8].

Before this understanding of the non-perturbative nature of the pseudospin symmetry, the condition $\Sigma'(r) = 0$, which appears in the pseudospin-orbital term, was interpreted as favoring the restoration of pseudospin symmetry due its competition with the centrifugal barrier [9]. For exotic nuclei with highly diffuse potentials, $\Sigma'(r) \approx 0$ may be a good approximation and then the pseudospin symmetry will be good [10]. In this case, to study exotic nuclei, it is necessary to use a Relativistic Continuum Hartree Bogoliubov (RCHB) theory that properly considers the pairing correlations and the coupling to the continuum via the Bogoliubov transformation in a microscopic and self-consistent way [10]. This approach is also useful when studying exotic nuclei with unusual N/Z ratios, where the neutron (or proton) Fermi surface is close to the particle continuum. The contribution of the continuum and/or resonances is then important [11]. In ref. [12], the pseudospin symmetry of the resonant states in ^{208}Pb was calculated by solving the Dirac equation with Woods-Saxon-like vector and scalar potentials using the coupling-constant method. It was found that the diffusivity of the potentials plays a significant role in the energy splitting and the width of the resonant pseudospin partners. In ref. [13], the pseudospin symmetry in single particle resonant states in nuclei was also shown to be exactly conserved under the same condition as for the pseudospin symmetry in bound states, i.e., $\Sigma(r) = 0$ or $\Sigma'(r) = 0$.

It is well accepted that RCHB theory can be used to study pairing correlations due to the short-range part of the nucleon-nucleon interaction in open shell nuclei, as well as to describe the exotic nuclei. However, the calculations of finite nuclei can be better performed when the pairing correlations, the nucleon, and mesons mean fields are all calculated self-consistently and this is not done for the pairing field in RCHB calculations, where the pairing correlation is introduced in a non-relativistic way as a Skyrme-type δ -force or finite range Gogny force [10]. In ref. [14] the self-consistent Dirac-Hartree-Bogoliubov (DHB) approach was introduced to self-consistently include pairing energy and gaps in calculations for spherical and deformed nuclei. As an extension, we have applied the DHB approach to hot nuclei

including finite temperature effects, to study spherical and deformed nuclei and to analyze how the binding energy, the neutron and charge radii, the deformation and, in particular, the pairing gap change with temperature [15]. We introduce in our finite temperature DHB (FTDHB) calculation a vapor subtraction procedure to take into account the contribution of the resonant nucleon states and to remove long range Coulomb repulsion between the hot nucleus and the gas as well as the contribution of the external nucleon gas [16–18]. Quite recently, we found that for small temperatures the vapor subtraction procedure is not very relevant to the change of the pairing fields with increasing temperature because the critical superfluidity and superconducting phase transitions occur at $T \sim 1$ MeV. The effects of the vapor phase that takes into account the unbound nucleon states become important only at temperatures $T \geq 4$ MeV, allowing the study of nuclear properties of finite nuclei from zero to high temperatures [19].

As in RCHB theory, the advantage of FTDHB to study pseudospin symmetry is that the particle levels for the bound states in the canonical basis are the same as those coming from solving the Dirac equation with scalar and vector potentials from RMF [10]. The form of the radial equations for the lower and upper components of the Dirac equation remain the same in the canonical basis even after the pairing interaction has been taken into account [10]. Furthermore, another advantage of FTDHB calculations lies in the fact that it considers the proper isospin dependence of the spin-orbit term, as well as the isospin and energy dependence of the pseudospin symmetry [10]. In non-selfconsistent RMF calculations the isospin asymmetry of the nuclear pseudospin comes mainly from the vector-isovector V_ρ potential and its effect on different terms of the Schrödinger-like equation contributing to the pseudospin splittings cancel each other to a certain extent [20]. On the other hand, the density dependence of the self-consistent relativistic mean fields and pairing fields, as well as the vapor phase that considers the unbound nucleon states, allows us to analyze in a realistic way the effect of temperature on the quasi degeneracy of pseudospin partners.

In this work, we use FTDHB calculations to study the temperature dependence of mean field potentials and its effects on pseudospin symmetry. The attractive scalar $V_S(r)$ and repulsive vector $V_V(r)$ potentials obtained in our calculations have a shape very similar to a Woods-Saxon one. We fit the central potential Σ_c mean field, as well as the total potential for neutrons and protons with a Woods-Saxon shape for each tin isotope in order to better assess how temperature changes the Woods-Saxon parameters: the depth of potential, the radius

R and the surface diffuseness a . In Relativistic Mean Field (RMF) theory at temperature zero, there is a correlation between the pseudospin-orbit term and the pseudospin energy splitting when the radius, diffusivity and the depth of potential are varied [7, 8, 20]. We will show that the degeneracy of pseudospin doublets decrease with increasing temperature and the behavior of parameters of Woods-Saxon potential for $T \neq 0$ obeys the same systematics as for $T = 0$.

We use the tin nuclei as a function of the number of nucleons from $A = 100$ to 170 and temperatures varying from $T = 0$ up to $T = 8$ MeV. These tin isotopes range allow us to apply our study to the stable and also unstable nuclei from proton drip line to the neutron drip line. The pseudospin symmetry was investigated before in these exotic nuclei using a RCHB calculation but at $T = 0$ [9]. For $T \neq 0$ these nuclei were also used to study the evolution of the pairing gaps and critical temperature along isotopic and isotonic chains of semimagic nuclei in FTDHB [19] and FTRHFB [21] calculations.

The paper is organized as follows. In sec. II we present briefly the formalism of the finite temperature Dirac-Hartree-Bogoliubov model. In sec. III we present and discuss the results of the calculations and in sec. IV we draw our conclusions.

II. THE FORMALISM

We use the self-consistent Dirac-Hartree-Bogoliubov (DHB) formalism of ref. [14], but consider explicitly the self-consistent temperature dependence of the relativistic pairing fields, as well as the vapor phase, to take into account the unbound nucleon states. This finite temperature DHB (FTDHB) formalism was developed in an earlier work [19] and includes the Coulomb and mesons mean fields, as well as pairing correlations, to calculate the properties of hot nuclei self-consistently. The Fock terms are neglected. The Hamiltonian form is given by

$$\begin{pmatrix} \varepsilon + \mu_t - h_t(\vec{x}) & \bar{\Delta}_t^\dagger(\vec{x}) \\ \bar{\Delta}_t(\vec{x}) & \varepsilon - \mu_t + h_t(\vec{x}) \end{pmatrix} \begin{pmatrix} \mathcal{U}_t(\vec{x}) \\ \gamma_0 \mathcal{V}_t(\vec{x}) \end{pmatrix} = 0, \quad t = p, n, \quad (1)$$

where, in the diagonal terms, ε denotes the quasi-particle energies, μ_t represents the chemical potential to be used as a Lagrange multiplier to fix the average number of protons ($t = p$) and neutrons ($t = n$), and h_t stands for the single-particle Hamiltonian of the nucleon.

The non-diagonal terms, $\overline{\Delta}_t$ and its conjugate $\overline{\Delta}_t^\dagger$, are the pairing fields, which account for correlated pairs of time-reversed single-particle states, i.e, the paired particle-particle states. The components $\mathcal{U}_t(\vec{x})$ and $\mathcal{V}_t(\vec{x})$ represents the Dirac spinors corresponding to the normal and time reversed components, respectively. We write each of the four-component spinors as

$$\mathcal{U}_{t\alpha}(\vec{x}) = \begin{pmatrix} G_{\mathcal{U},t\alpha}(\vec{x}) \\ i F_{\mathcal{U},t\alpha}(\vec{x}) \end{pmatrix}, \quad \text{and} \quad \gamma_0 V_{t\alpha}(\vec{x}) = \begin{pmatrix} G_{\mathcal{V},t\alpha}(\vec{x}) \\ i F_{\mathcal{V},t\alpha}(\vec{x}) \end{pmatrix}. \quad (2)$$

The Dirac Hamiltonian is

$$h_t(\vec{x}) = -i\vec{\alpha} \cdot \vec{\nabla} + \beta M^*(\vec{x}) + V_t(\vec{x}), \quad (3)$$

where the effective mass M^* contains the scalar part of the nucleon self-energy from the Dirac field and V_t is the vector potential. These are written as

$$M^*(\vec{x}) = M - g_\sigma \sigma(\vec{x}) \quad (4)$$

$$V_t(\vec{x}) = g_\omega \omega^0(\vec{x}) + \frac{g_\rho}{2} 2m_t \rho^{00}(\vec{x}) + e \left(\frac{1}{2} + m_t \right) A^0(\vec{x}). \quad (5)$$

The constant M is the nucleon mass, while g_σ , g_ω , g_ρ , and e are the corresponding coupling constants for the mesons and the photon. The isospin projections are $m_t = 1/2$ for protons and $m_t = -1/2$ for neutrons. The fields ω^0 and A^0 are the time-like components of the four-vector ω and photon fields, while ρ^{00} is the third component of the time-like component of the isovector-vector ρ meson,

$$\begin{aligned} \omega^0(\vec{x}) &= g_\omega \int d^3z d_\omega^0(\vec{x} - \vec{z}) \rho_B(\vec{z}), \\ \rho^{00}(\vec{x}) &= \frac{g_\rho}{2} \int d^3z d_\rho^0(\vec{x} - \vec{z}) \rho_3(\vec{z}), \\ A^0(\vec{x}) &= e \int d^3z d_\gamma^0(\vec{x} - \vec{z}) \rho_c(\vec{z}), \\ \sigma(\vec{x}) &= g_\sigma \int d^3z d_\sigma(\vec{x} - \vec{z}) \rho_s(\vec{z}) \\ &= \int d^3z d_\sigma^0(\vec{x} - \vec{z}) (g_\sigma \rho_s(\vec{z}) - g_3 \sigma(\vec{x})^2 - g_4 \sigma(\vec{x})^3). \end{aligned} \quad (6)$$

where the propagators are

$$d_j^0(\vec{x} - \vec{z}) = \frac{1}{4\pi |\vec{x} - \vec{z}|} \times \begin{cases} 1 & , \text{ for photon} \\ \exp(-m_j |\vec{x} - \vec{z}|) & , \text{ for mesons} \end{cases} \quad (7)$$

The Hartree contributions to the self-energy can be written in terms of the normal densities,

$$\begin{aligned} \rho_s(\vec{x}, T) &= 2 \sum_{\varepsilon_{t\alpha} < 0, t} \left(\mathcal{U}_{t\alpha}^\dagger \gamma_0 \mathcal{U}_{t\alpha} n(\varepsilon_{t\alpha}, T) + \mathcal{V}_{t\alpha}^\dagger \gamma_0 \mathcal{V}_{t\alpha} n(-\varepsilon_{t\alpha}, T) \right), \\ \rho_B(\vec{x}, T) &= 2 \sum_{\varepsilon_{t\alpha} < 0, t} \left(\mathcal{U}_{t\alpha}^\dagger \mathcal{U}_{t\alpha} n(\varepsilon_{t\alpha}, T) + \mathcal{V}_{t\alpha}^\dagger \mathcal{V}_{t\alpha} n(-\varepsilon_{t\alpha}, T) \right), \\ \rho_3(\vec{x}, T) &= 2 \sum_{\varepsilon_{t\alpha} < 0, t} 2m_t \left(\mathcal{U}_{t\alpha}^\dagger \mathcal{U}_{t\alpha} n(\varepsilon_{t\alpha}, T) + \mathcal{V}_{t\alpha}^\dagger \mathcal{V}_{t\alpha} n(-\varepsilon_{t\alpha}, T) \right), \\ \rho_c(\vec{x}, T) &= 2 \sum_{\varepsilon_{t\alpha} < 0, t} (m_t + 1/2) \left(\mathcal{U}_{t\alpha}^\dagger \mathcal{U}_{t\alpha} n(\varepsilon_{t\alpha}, T) + \mathcal{V}_{t\alpha}^\dagger \mathcal{V}_{t\alpha} n(-\varepsilon_{t\alpha}, T) \right). \end{aligned} \quad (8)$$

The Hamiltonian form of the pairing field is,

$$\begin{aligned} \bar{\Delta}_t^\dagger(\vec{x}) &= \gamma_0 \Delta_t(\vec{x}) \gamma_0 \\ &= c_{pair} \left(\frac{g_\sigma^2}{m_\sigma^2} \gamma_0 \kappa_t(\vec{x}, T) \gamma_0 \right. \\ &\quad \left. - \left(\frac{g_\omega^2}{m_\omega^2} + \frac{(g_\rho/2)^2}{m_\rho^2} \right) \gamma_0 \gamma^\mu \kappa_t(\vec{x}, T) \gamma_\mu \gamma_0 \right). \end{aligned} \quad (9)$$

where we neglect its Coulomb and nonlinear σ -meson contributions. We approximate the contributions of the other mesons using the zero-range limit of the meson propagators. The zero-range approximation greatly simplifies the numerical calculations, but must be calibrated phenomenologically. Thus, an overall constant c_{pair} has been introduced in the expression for the pairing field to compensate for deficiencies of the interaction parameters and of the numerical calculation [14, 19]. The anomalous density $\kappa_t(\vec{x}, T)$ is given by

$$\begin{aligned} \kappa_t(\vec{x}, T) &= \frac{1}{2} \sum_{\varepsilon_{t\gamma} < 0} \left(\mathcal{U}_{t\gamma}(\vec{x}) \bar{\mathcal{V}}_{t\gamma}(\vec{x}) + \gamma_0 B \mathcal{V}_{t\gamma}^*(\vec{x}) \mathcal{U}_{t\gamma}^T(\vec{x}) B^\dagger \right) \\ &\quad \times (n(\varepsilon_{t\gamma}, T) - n(-\varepsilon_{t\gamma}, T)), \end{aligned} \quad (10)$$

where $B = \gamma_5 C$ and C is the charge conjugation matrix that provides the time-reversed Dirac structure of the wave vectors.

For both normal and anomalous densities, one sees that the temperature enters in our

calculation only through the Fermi occupation factors

$$n(\varepsilon_\gamma, T) = \frac{1}{1 + \exp(\varepsilon_\gamma/T)}, \quad (11)$$

where ε_γ represent the quasi-particle energy. Thus, the temperature dependence of a solution of the FTDHB equation comes from the quasi-particle normal and anomalous densities. When $T \rightarrow 0$, the Fermi occupation factors are $n(\varepsilon_\gamma, T) = 1$ and $n(-\varepsilon_\gamma, T) = 0$ and we recover the usual nuclear densities of a finite nucleus. The quasi-particle energies that enter each Fermi occupation factor have opposite signs. Thus, as T increases, there is a reduction of the anomalous density due to the difference between the two contributions to the Fermi occupation factor, as we see in Eq. (10). As a consequence the pairing energy and gap tend to zero as the temperature increases [19].

Specifically for axially-symmetric potentials the scalar and vector potential are independent of the azimuthal angle such that $V_{S,V} = V_{S,V}(r_\perp, z)$. We have that $V_{S,V}(r_\perp, z) \rightarrow 0$ for $r_\perp \rightarrow \infty$ or $z \rightarrow \pm\infty$, and $r_\perp V_{S,V}(r_\perp, z) \rightarrow 0$ for $r_\perp \rightarrow 0$ [22]. Furthermore, the rotational symmetry is broken when we chose this axial symmetry, but the densities are invariant with respect to a rotation around the symmetry axis. As a consequence the projection of the total angular momentum along the symmetry axis Ω_α , as well as the parity π and the isospin projection t , are still good quantum numbers. Due to this fact and the time-reversed Dirac structure, the two equal and opposite values of angular momentum projection $\pm\Omega_\alpha$ are degenerate in energy.

The Dirac spinors in Eqs. (2) takes the form

$$\mathcal{U}_{t\alpha}(\vec{x}) = \frac{1}{\sqrt{2\pi}} \begin{pmatrix} G_{\mathcal{U},t\alpha}^+(r_\perp, z) e^{i(\Omega_\alpha-1/2)\varphi} \\ G_{\mathcal{U},t\alpha}^-(r_\perp, z) e^{i(\Omega_\alpha+1/2)\varphi} \\ i F_{\mathcal{U},t\alpha}^+(r_\perp, z) e^{i(\Omega_\alpha-1/2)\varphi} \\ i F_{\mathcal{U},t\alpha}^-(r_\perp, z) e^{i(\Omega_\alpha+1/2)\varphi} \end{pmatrix} \quad (12)$$

and

$$\gamma_0 V_{t\alpha}(\vec{x}) = \frac{1}{\sqrt{2\pi}} \begin{pmatrix} G_{\mathcal{V},t\alpha}^+(r_\perp, z) e^{i(\Omega_\alpha-1/2)\varphi} \\ G_{\mathcal{V},t\alpha}^-(r_\perp, z) e^{i(\Omega_\alpha+1/2)\varphi} \\ i F_{\mathcal{V},t\alpha}^+(r_\perp, z) e^{i(\Omega_\alpha-1/2)\varphi} \\ i F_{\mathcal{V},t\alpha}^-(r_\perp, z) e^{i(\Omega_\alpha+1/2)\varphi} \end{pmatrix}. \quad (13)$$

Thus, the radial wave functions $G_{u,v}^{\pm}(r_{\perp}, z)$ and $F_{u,v}^{\pm}(r_{\perp}, z)$ and the meson fields are expanded in terms of the eigenfunctions of a deformed axially symmetric harmonic oscillator:

$$V_{osc}(z, r_{\perp}) = \frac{1}{2}M(\omega_z^2 z^2 + \omega_{\perp}^2 r_{\perp}^2) \quad (14)$$

where the oscillator frequencies $\hbar\omega_z$ and $\hbar\omega_{\perp}$ are written in terms of a deformation parameter β_0 , as

$$\hbar\omega_z = \hbar\omega_0 e^{-\sqrt{5/(4\pi)}\beta_0} \quad \text{and} \quad \hbar\omega_{\perp} = \hbar\omega_0 e^{+\frac{1}{2}\sqrt{5/(4\pi)}\beta_0}. \quad (15)$$

The (z, r_{\perp}) -dependence of eigenfunctions in large and small components of the Dirac spinors are divided by oscillator length,

$$b_z = \sqrt{\hbar/M\omega_z} \quad \text{and} \quad b_{\perp} = \sqrt{\hbar/M\omega_{\perp}}, \quad (16)$$

and due of volume conservation it is guaranteed $b_z b_{\perp}^2 = b_0^3$. The parameter $b_0 = \sqrt{\hbar/M\omega_0}$ stands for the oscillator length corresponding to the oscillator frequency $\hbar\omega_0$ of the spherical case. In this way the spherical and deformed basis are determined by oscillator frequency $\hbar\omega_0$ and deformation β_0 . Thus the method can be applied to both spherical and axially deformed nuclei.

Inserting these expansions of eigenfunctions into the Dirac-Gorkov equation Eq. (1), we can reduce the equation to the diagonalization problem of a symmetric matrix and calculate the Hartree densities of Eq. (8) and the components of the anomalous density of Eq. (9). The fields of the massive mesons are obtained by solving the Klein-Gordon equations using a similar expansion with the same deformation parameter β_0 but a smaller oscillator length of $b_B = b_0/\sqrt{2}$. The Coulomb field is calculated directly in configuration space.

This method is a direct generalization of the one described in refs. [14, 19, 23–26] where more details can be found.

III. RESULTS

In this section we present FTDHB calculations for hot nuclei to investigate the effect of temperature in the mean field potentials and its consequences for the pseudospin symmetry. To study the effect of temperature in the mean field potentials we examine the tin isotopes

from $A = 100$ to $A = 170$. We use the nonlinear Walecka model with the NL3 interactions. In our calculations, the expansion of harmonic oscillator basis is truncated at a finite number of major shells, with the quantum number of the last included shell set by $N_F = 14$ in the case of the fermions and by $N_B = 24$ for the bosons. These bases are sufficient to achieve convergence in our numerical calculation and reproduce experimental and earlier theoretical results of the literature at both low and high temperatures. In all cases, the oscillator frequencies $\hbar\omega_0 = \hbar\omega_z = \hbar\omega_\perp = 41A^{-1/3}$ MeV, corresponding to an undeformed basis, were used. A value of the overall constant $c_{pair} = 0.55$ was introduced in the pairing interaction for neutrons and protons, Eq. (9), which due to the self-consistency, results in a null pairing field, as expected for the closed-shell nuclei we are studying. This means we are studying the spherical tin isotopes from $A = 100$ to $A = 170$. Among them, the nuclei ^{100}Sn , ^{132}Sn , and ^{176}Sn have pairing gap and energy zero, so that pairing has no effect on pseudospin symmetry over the entire range of temperatures considered. For open-shell and deformed nuclei, the nuclear pairing energy and gap vanishes above the relatively low temperatures of $T = 0.5 - 1.2$ MeV [19, 21].

In Fig. 1(a) we show the potentials $V_\rho(r)$, $\Sigma_c(r) = V_\sigma(r) + V_\omega(r)$, and $V_n(r) = \Sigma_c(r) - V_\rho(r)$, as a function of the radial distance for ^{100}Sn and ^{150}Sn at $T = 0$. The full lines represent the nucleus ^{100}Sn , for which we see that the $V_\rho(r)$ potential (empty squares) is very small, while its sum with $\Sigma_c(r)$ (empty circles) produces a shallow potential $V_n(r)$ (full circles) for neutrons. The same behavior can be seen for ^{150}Sn , represented by the dashed lines, but now $V_\rho(r)$ is large and as a consequence $V_n(r)$ is more affected by it. In Fig. 1(b), the $V_\rho(r)$ potential has the opposite sign, the repulsive Coulomb potential $V_{coul}(r)$ has a long range and their sum shifts the potential $V_p(r) = \Sigma_c(r) + V_\rho(r) + V_{coul}(r)$ for protons. Because of the small $V_\rho(r)$ potential in comparison to $V_{coul}(r)$ for ^{100}Sn , the large difference between $V_p(r)$ and $\Sigma_c(r)$ at the nuclear center is due practically to $V_{coul}(r)$ alone. For ^{150}Sn , the contribution of $V_\rho(r)$ is significant in comparison to $V_{coul}(r)$, and as a consequence there is a cancellation between the two that produces a difference of the same order of magnitude between $V_p(r)$ and $\Sigma_c(r)$. In the DHB calculation, the nuclear potentials for protons and neutrons for the case $N = Z$ (^{100}Sn) are not the same. The Coulomb potential changes the proton energy levels and, because of that, in the self-consistent DHB calculation the neutron energy levels are also changed in such a way that there is a net V_ρ potential [20].

In Fig. 1(c) we show the potential $V_n(r)$ for neutrons and in Fig. 1(d) the potential

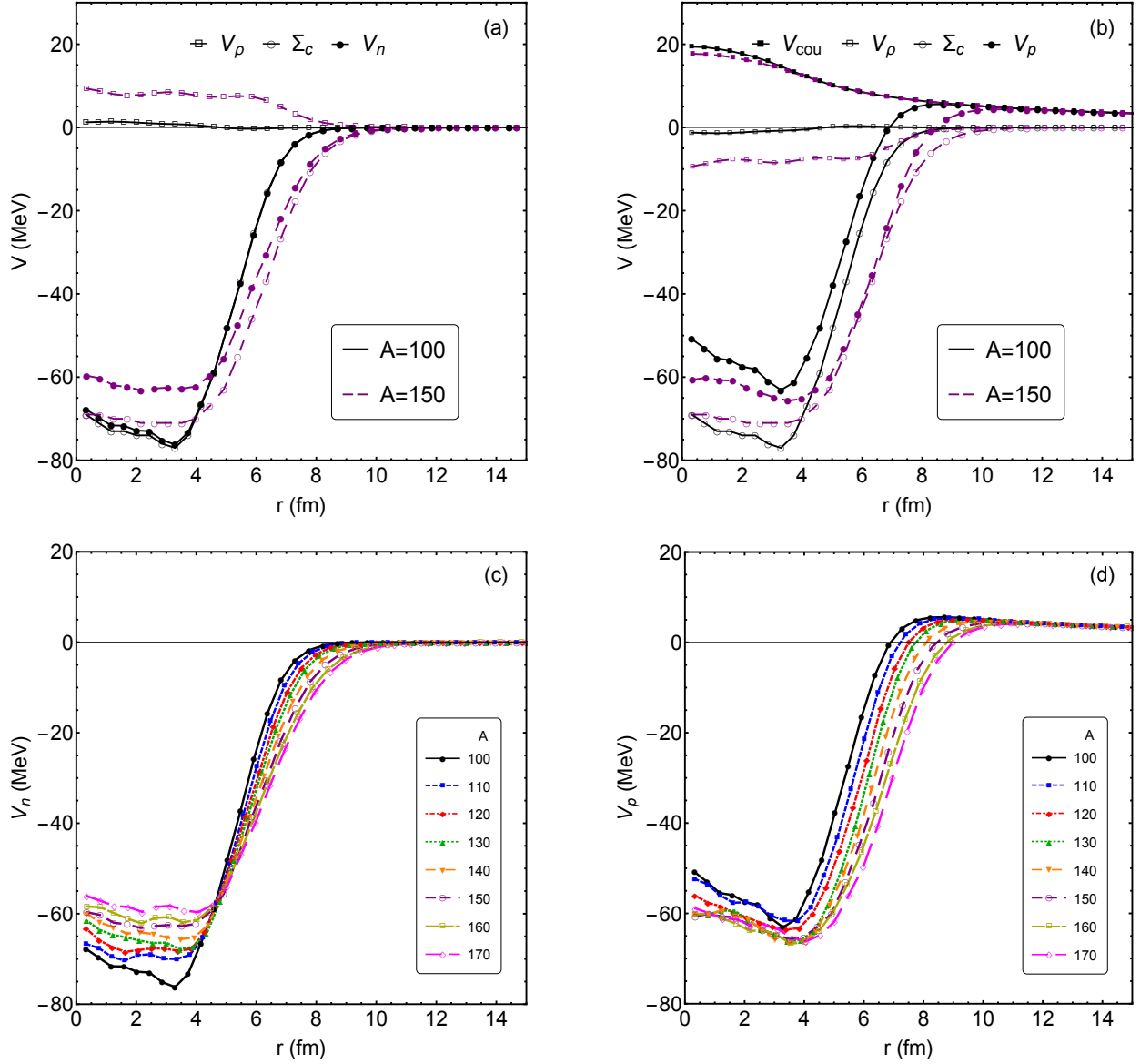


FIG. 1. (Color online) Nuclear potentials as a function of the radial distance for the tin isotope chain. In the top panels, the meson potentials for (a) neutrons and (b) protons with the Coulomb potential are displayed for ^{100}Sn (full lines) and ^{150}Sn (dashed lines). In the bottom panels, the potentials (c) $V_n(r)$ for neutrons and (d) $V_p(r)$ for protons are shown from $A = 100$ to $A = 170$.

$V_p(r)$ for protons as a function of radial distance for the tin isotope chain from $A = 100$ to $A = 170$. These results, obtained in a FTDHB self-consistent calculation, show that the mean field potentials have the shape of a Woods-Saxon potential. In refs. [7, 8] RMF studies at $T = 0$ were performed to investigate the correlation between the pseudospin splitting and the parameters of the Wood-Saxon potential: its depth (Σ_0), surface diffuseness (a), and radius (R). In ref. [20] this was done for a single isotope chain. The neutron $V_n(r)$ and proton $V_p(r)$ mean field potentials in a tin isotope chain were parametrized by a Woods-

Saxon form as functions of A . For the tin isotopes as A increases, the central potential $|\Sigma_0|$ decreases and the surface diffuseness increases, effects which both favor the pseudospin symmetry. However, the radius increases with A , which can partially offset those effects [7]. Since the values $|\Sigma_0|R^2$ are roughly constant for neutrons, the correlation between these two values, mentioned above, implies that the effects of increasing R and decreasing $|\Sigma_0|$ in the neutron central potential, when A increases, balance each other. Thus, the dominant effect comes from the increasing value of a , slightly favoring the pseudospin symmetry [20]. However, for protons, the value $|\Sigma_0|R^2$ is not constant, because both $|\Sigma_0|$ and the radius R increase as A increases for the tin isotopes. Hence, the changes in $|\Sigma_0|$ and R disfavor the pseudospin symmetry in this case. The isospin asymmetry in pseudospin symmetry is due to the isovector V_ρ potential, which is repulsive for neutrons and attractive for protons and makes the vector potential V_V bigger for neutrons than for protons. As a consequence, $|\Sigma_0|$ becomes smaller for neutrons than for protons [7, 20].

In order to study the same effect at finite temperature, we will fit the self-consistent potentials $\Sigma_c(r)$, $V_n(r)$, and $V_p(r)$ to a Woods-Saxon shape for $T \neq 0$. In the left column of Fig. 2 we show our FTDHB calculations of the (a) $\Sigma_c(r)$, (c) $V_n(r)$, (e) and $V_p(r)$ potentials as a function of the radial distance for the nucleus ^{100}Sn , in equilibrium with the external gas, as the temperature varies from $T = 0$ to $T = 8$ MeV. At $T = 0$ the $\Sigma_c(r)$ (in Fig. 2(a)) and $V_n(r)$ (in Fig. 2(c)) potentials vanish at the surface. When the temperature is increased, these potentials no longer go to zero at large radii because of the contribution of the gas consisting of nucleons that evaporate for $T \neq 0$. We show the potential $V_p(r)$ (in Fig. 2(e)) for protons in ^{100}Sn over the same range of the temperatures. The proton potential vanishes at a larger radius than the neutron one because of the long-range effect of the Coulomb potential. In our calculations, we use the Bonche, Levit, and Vautherin procedure to take into account the evaporated nucleons that become important at temperatures above about 3 – 4 MeV [16, 17]. Note that beyond about $T \geq 8$ MeV, the nuclear structure is almost completely dissolved since the stability of a hot nucleus depends on maintaining the balance between surface and Coulomb contributions, as discussed in refs. [16–19].

To study the effect of temperature on pseudospin symmetry and its possible causes, and in view of the systematics uncovered in ref. [20] referred to above, we study the change in shape of the self-consistent mean fields with temperature, which appears as changes with temperature of the Woods-Saxon parameters of the fitted potentials, namely their depth

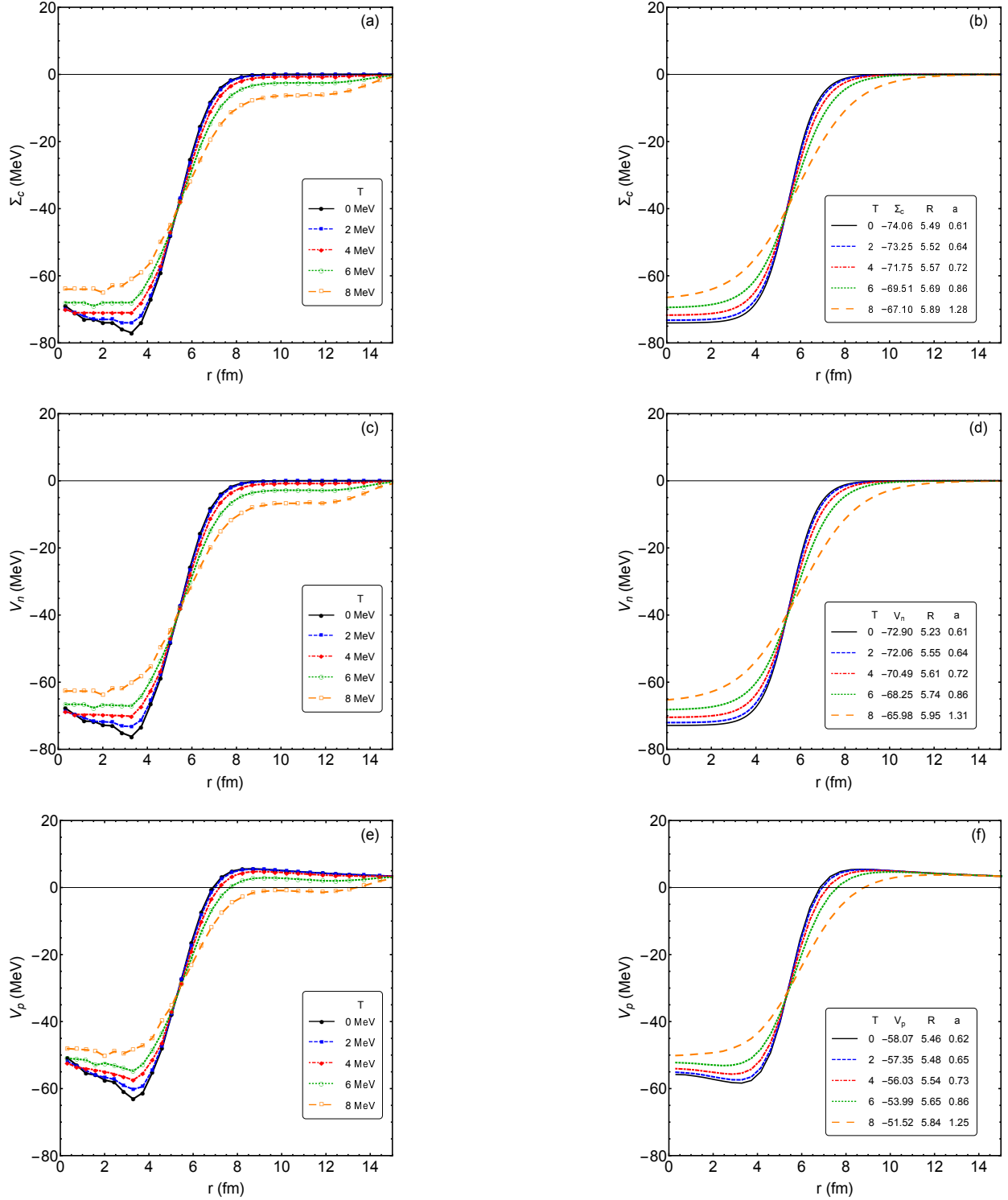


FIG. 2. (Color online) Nuclear potentials of the nucleus ^{100}Sn as a function of the radial distance with temperatures varying from $T = 0$ to $T = 8$ MeV. The left column represents our FTDHB calculations for (a) $\Sigma_c(r)$, (c) $V_n(r)$, and (e) $V_p(r)$. The right column shows our fit with a Woods-Saxon shape of the (b) $\Sigma_c(r)$, (d) $V_n(r)$, and (f) $V_p(r)$, together with the Woods-Saxon parameters depth V_0 (in MeV), radius R (in fm), and surface diffuseness a (in fm).

(V_0), radius (R), and diffusivity (a). We show in the right column of Fig. 2 our fit with a Woods-Saxon shape of the (b) $\Sigma_c(r)$, (d) $V_n(r)$, and (f) $V_p(r)$ potentials of the nucleus ^{100}Sn , together with the values of the corresponding Wood-Saxon parameters, for temperatures varying from $T = 0$ to $T = 8$ MeV. The fit is good for temperatures $T \leq 8$ MeV and the Bonche, Levit, and Vautherin procedure can be considered adequate for our calculations in this temperature range. In the right column of Fig. 2 we can read the Woods-Saxon parameters in the legend of each subfigure. We observe that, as the temperature increases, the depths of the potentials decrease while their radii and surface diffuseness parameters increase. The depth of the potentials decreases about $\sim 10\%$ between $T = 0$ and $T = 8$ MeV as the radii increase in about the same ratio of $\sim 10\%$. However, the diffusivities increase at least 50% or more over the same range of temperatures. The same studies were performed for ^{132}Sn and ^{150}Sn with similar results.

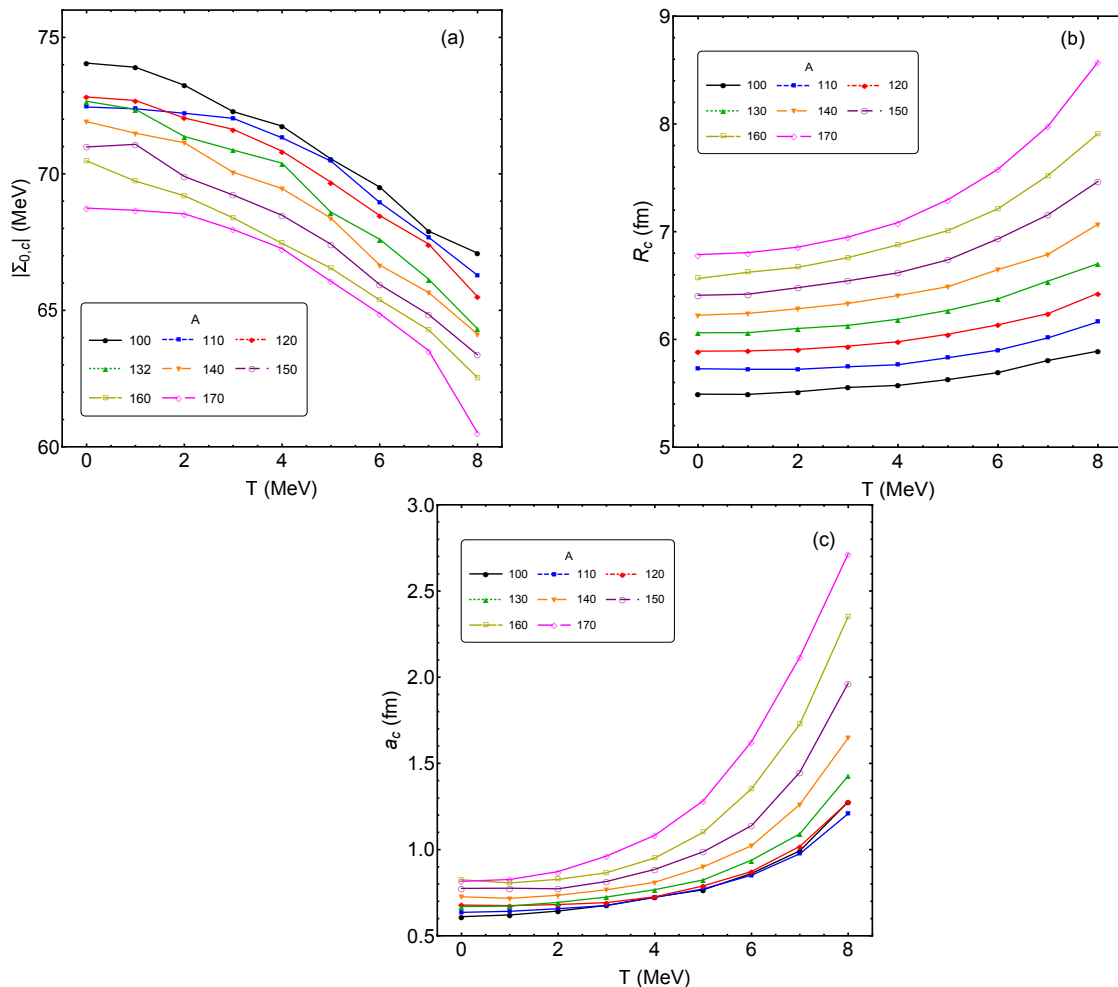


FIG. 3. (Color online) The Woods-Saxon potential parameters for the (a) depth $|\Sigma_{0,c}|$, (b) radius R_c , and (c) diffusivity a_c , versus temperature for tin isotope chain.

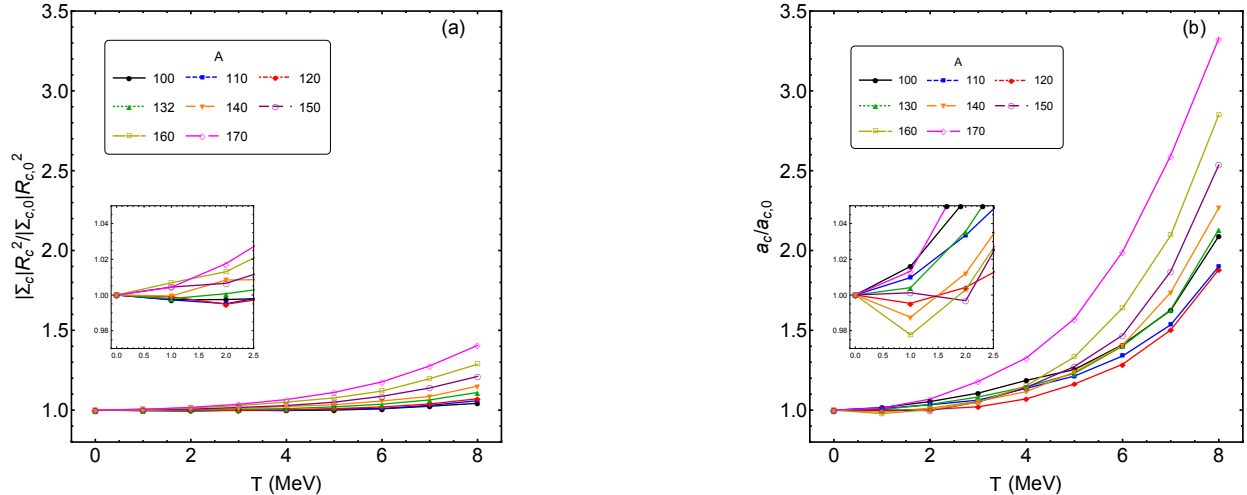


FIG. 4. (Color online) The Woods-Saxon parameters (a) $|\Sigma_c|R_c^2$, and (b) diffusivity a_c divided by their respective values at $T = 0$, versus temperature for the tin isotope chain.

One can conclude from these figures that when the temperature increases the central depth Σ_0 decreases and the radius and the surface diffuseness increase. To see this more clearly, in Fig. 3 we show the Woods-Saxon parameters for the tin isotopes as the temperature increases up to the limit $T = 8$ MeV. In Fig.3(a) the value of $|\Sigma_{0,c}|$ decreases as the temperature increases. In Fig. 3(b) we show that the radius R_c also increases with temperature. However, as we see in Fig. 3(c) the surface diffuseness increases quickly with increasing temperature. When we fix a value of the temperature, the value of $|\Sigma_{0,c}|$ decreases as A increases, while both the radius R_c and surface diffuseness a_c increase as A increases. In fact, these results are expected due to the known $A^{1/3}$ dependence of the nuclear radius. Our results agree with calculations of the RMF theory at $T = 0$ [7, 8].

This opposing tendency of $|\Sigma_c|$ and R produces values of $|\Sigma_c|R_c^2$ that are roughly constant for each isotope from $T = 0$ to $T = 8$ MeV. In Fig. 4 we show the product $|\Sigma_c|R_c^2$ over $|\Sigma_{c,0}|R_{c,0}^2$ at $T = 0$ for tin isotopes as the temperature increases. The ratio is almost constant and changes very little below $T = 8$ MeV. In Fig. 4(b) we show that diffuseness a_c over $a_{c,0}$ at $T = 0$ also increases with temperature, but this change is very large up to $T = 8$ MeV in comparison to that seen in Fig. 4(a).

Summarizing, as T increases, the central depth $|\Sigma_0|$ decreases and the radius R increases, but both effects balance each other, since the values of $|\Sigma_0|R^2$ are roughly constant. Thus, when T increases, the dominant effect comes from the increasing diffuseness a , which favors the pseudospin symmetry as found in ref. [20].

In Table I we show the pseudospin partners of the neutrons and protons of ^{100}Sn . The magnitude of the neutron pseudospin energy splitting (Δ_n in MeV) decreases with increasing temperature. We also see that the pseudospin splitting also decreases for protons (Δ_p in MeV). However, for protons, the pseudospin splitting is larger than for neutrons, at least for the deep doublet $[2s_{1/2} - 1d_{3/2}]$ of the symmetric nucleus ^{100}Sn .

TABLE I. Pseudospin energy splitting in MeV of the pseudospin partners of ^{100}Sn for neutrons (Δ_n) and protons (Δ_p) at several values of the temperature T in MeV.

T	$2s_{1/2}$	$1d_{3/2}$	Δ_n	$2p_{3/2}$	$1f_{5/2}$	Δ_n	$2s_{1/2}$	$1d_{3/2}$	Δ_p	$2p_{3/2}$	$1f_{5/2}$	Δ_p
0	34.38	38.74	4.36	20.94	24.23	3.29	19.25	23.74	4.49	6.44	9.64	3.20
1.0	34.38	38.60	4.22	20.97	24.18	3.21	19.28	23.63	4.36	6.49	9.62	3.13
2.0	34.24	37.80	3.56	21.01	23.81	2.79	19.32	23.03	3.71	6.69	9.45	2.75
3.0	33.87	37.06	3.19	20.93	23.46	2.52	19.17	22.50	3.33	6.82	9.30	2.48
4.0	33.45	36.38	2.93	20.87	23.14	2.27	18.95	22.01	3.06	6.96	9.18	2.22
5.0	33.00	35.62	2.62	20.88	22.81	1.93	18.73	21.47	2.74	7.19	9.07	1.88
6.0	32.43	34.70	2.27	20.90	22.45	1.55	18.47	20.83	2.37	7.50	9.00	1.50
7.0	31.69	33.56	1.87	20.87	22.03	1.15	18.12	20.07	1.95	7.85	8.95	1.10
8.0	30.74	32.10	1.36	20.76	21.42	0.67	17.68	19.10	1.42	8.25	8.85	0.60

In Table II we show the neutron pseudospin partners of ^{150}Sn . The magnitude of the pseudospin splitting increases up to $T = 2$ MeV and then begins to decrease with the temperature for the deeper doublets. The splitting of the doublet $[2f_{7/2} - 1h_{9/2}]$ has the opposite sign and its magnitude decreases up to $T = 3$ MeV and then starts to increase with temperature. In Table III we show the proton pseudospin partners of ^{150}Sn . The magnitude of the pseudospin splitting of the doublets $[2p_{3/2} - 1f_{5/2}]$ and $[2d_{5/2} - 1g_{7/2}]$ increases up to $T = 2$ MeV and then starts to decrease. The splitting of the doublets $[2s_{1/2} - 1d_{3/2}]$ and

TABLE II. Pseudospin energy splitting for neutrons (Δ_n) in MeV for pseudospin partners of ^{150}Sn for several values of T in MeV.

T	$2s_{1/2}$	$1d_{3/2}$	Δ_n	$2p_{3/2}$	$1f_{5/2}$	Δ_n	$2d_{5/2}$	$1g_{7/2}$	Δ_n	$2f_{7/2}$	$1h_{9/2}$	Δ_n
0	32.91	35.78	2.87	21.93	24.66	2.73	11.79	13.29	1.50	3.11	2.52	-0.59
1.0	32.83	35.73	2.90	21.87	24.67	2.79	11.77	13.34	1.57	3.12	2.59	-0.53
2.0	32.62	35.57	2.94	21.79	24.71	2.91	11.85	13.54	1.69	3.32	2.90	-0.42
3.0	32.31	35.20	2.89	21.74	24.57	2.83	12.06	13.66	1.59	3.73	3.27	-0.46
4.0	31.87	34.63	2.75	21.69	24.31	2.62	12.37	13.77	1.40	4.31	3.77	-0.55
5.0	31.29	33.81	2.52	21.60	23.91	2.31	12.73	13.87	1.14	5.04	4.37	-0.67
6.0	30.53	32.73	2.20	21.45	23.37	1.92	13.13	13.95	0.82	5.91	5.07	-0.83
7.0	29.51	31.32	1.81	21.17	22.64	1.47	13.54	14.00	0.47	6.93	5.91	-1.02
8.0	28.17	29.48	1.31	20.72	21.66	0.94	13.95	13.97	0.03	8.16	6.87	-1.30

$[2f_{7/2} - 1h_{9/2}]$ decreases with temperature already from $T = 0$. The doublet $[2d_{5/2} - 1g_{7/2}]$ is not populated at temperature $T = 0$ and $[2f_{7/2} - 1h_{9/2}]$ is populated only when $T \geq 2$ MeV. The non-occupied states at $T = 0$ are due to the temperature effect when we consider the Fermi occupation factor. If we analyze each pseudospin partner of Tables II and II, we see that the energy splitting is smaller for neutrons in comparison to protons, as expected from the isospin asymmetry of the pseudospin symmetry [7, 20].

TABLE III. Pseudospin energy splitting for protons (Δ_p) for the pseudospin partners of ^{150}Sn for several values of T .

T	$2s_{1/2}$	$1d_{3/2}$	Δ_p	$2p_{3/2}$	$1f_{5/2}$	Δ_p	$2d_{5/2}$	$1g_{7/2}$	Δ_p	$2f_{7/2}$	$1h_{9/2}$	Δ_p
0	33.10	36.57	3.47	22.29	25.61	3.31	-	-	-	-	-	-
1.0	33.13	36.60	3.47	22.32	25.69	3.37	11.87	14.35	2.48	-	-	-
2.0	33.14	36.51	3.37	22.39	25.85	3.46	12.02	14.70	2.69	2.25	3.69	1.43
3.0	33.00	36.25	3.24	22.46	25.81	3.35	12.32	14.92	2.60	2.80	4.16	1.37
4.0	32.77	35.84	3.07	22.57	25.71	3.14	12.77	15.18	2.41	3.59	4.79	1.20
5.0	32.45	35.29	2.83	22.71	25.55	2.84	13.35	15.49	2.13	4.61	5.58	0.97
6.0	32.01	34.52	2.51	22.82	25.29	2.47	14.02	15.80	1.79	5.82	6.49	0.67
7.0	31.32	33.44	2.12	22.82	24.84	2.03	14.70	16.07	1.37	7.20	7.50	0.30
8.0	30.29	31.92	1.62	22.62	24.09	1.47	15.36	16.19	0.83	8.78	8.55	-0.23

In Figure 5(a) we show several neutron pseudospin doublets of the nucleus ^{150}Sn . The energy splitting increases with temperature up to $T = 2$ MeV and then begins to decrease, except for the doublet $[3s_{1/2} - 2d_{3/2}]$, which decreases monotonically. In Figure 5(b) we show several proton pseudospin doublets of the nucleus ^{150}Sn . As we see there, the energy splitting also increases for the deeper levels up to $T = 2$ MeV and unoccupied states exist below this temperature for the upper levels. This behavior below $T = 2$ MeV is not consistently observed for other isotopes. This may be due to other effects, such as thermal or pairing effects, which might interfere with the direct competition between the surface diffusivity and $|\Sigma|R^2$. For temperatures below $T = 2$ MeV, the surface diffuseness a_c is almost constant while the product $|\Sigma_{c,0}|R_{c,0}^2$, increases slightly more for ^{150}Sn , as we see in the zoom inside Figures 4(a) and 4(b), respectively. These effects could furnish an increase in the pseudospin splitting up to $T = 2$ MeV. However, this behavior does not apply to other isotopes. However, for $T > 2$ MeV the energy splitting of the pseudospin doublets decreases as temperature increases. The exceptions are the two doublets $[2f_{7/2} - 1h_{9/2}]$ and $[3p_{3/2} - 2f_{5/2}]$ for neutrons that become more degenerate above $T \sim 3$ MeV. The increase of diffusivity with temperature determines the growth of the ratio $a_c/a_{c,0}$ larger in comparison

to the changes in $|\Sigma_c|R_c^2/|\Sigma_{c,0}|R_{c,0}^2$ induced by the temperature, favoring the pseudospin symmetry.

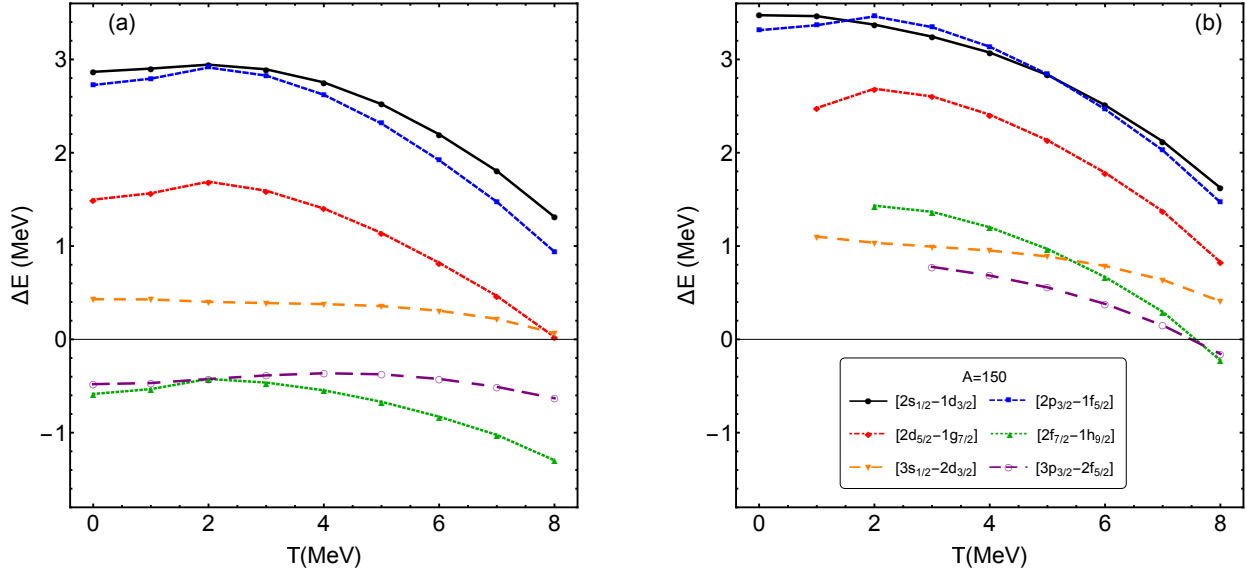


FIG. 5. (Color online) Energy splitting for several pseudospin doublets of ^{150}Sn for (a) neutrons and (b) protons for temperatures varying from $T = 0$ up to $T = 8$ MeV.

IV. CONCLUSION

In this work we have studied the effects of temperature on the energy splitting of several pseudospin doublets of the spherical tin isotopes. We used the finite temperature Dirac-Hartree-Bogoliubov (FTDHB) formalism to obtain the mean field and Coulomb potentials in a self-consistently calculation [19]. This formalism allows us to take into account the pairing and deformation beyond the mean field and Coulomb potentials. In our calculations, we observe that the mean field potentials have the shape of Woods-Saxon potentials for the temperature range from $T = 0$ MeV to $T = 8$ MeV. By fitting the potentials to Wood-Saxon potentials, we were able to investigate the correlation between the pseudospin splittings and the parameters of the Wood-Saxon potential: the depth (Σ_0), surface diffuseness (a), and radius (R). We studied the tin nuclei from $A = 100$ to $A = 170$ as a function of temperature between $T = 0$ and $T = 8$ MeV. For each nuclei we obtained the values of the parameters of the Wood-Saxon potential and analyzed their variation with increasing temperature. We found that for ^{100}Sn the depth of the potential decreases while the radius and surface

diffuseness increase with temperature. The depth of the potential decreases on the order of $\sim 10\%$ while the radius increases in the same ratio between $T = 0$ and $T = 8$ MeV. However, the diffusivity increases by at least $\sim 50\%$ in the same temperature range. The other tin isotopes show similar results. From the calculation of the energy splittings for the neutron and proton pseudospin partners of the tin isotopes at several values of the temperature, we see that in general the pseudospin energy splittings decrease with temperature. This confirms the systematics already found in ref. [20] for the tin isotopes at $T = 0$, in which the change in diffusivity was the main driver for the variation in pseudospin energy splittings, which favors pseudospin symmetry. The decrease of the energy difference between pseudospin doublets with the increase of the temperature seems also to be valid for deformed nuclei at large temperatures. In ref. [19] we show that ^{168}Er becomes spherical and the splitting decreases for temperature $T \geq 4$ MeV.

We can thus restate, now including the effects of temperature that, in general, there is a correlation between the shape of the nuclear mean-fields, described here by Wood-Saxon parameters, and the onset of pseudospin symmetry on nuclei.

ACKNOWLEDGMENTS

The authors acknowledge financial support from CAPES, CNPq, FAPESP and FAPERJ. R. L. acknowledges, in particular, support from the CNPq/FAPERJ/PRONEM:003/2011. M. M. acknowledges the financial support of CNPq and FAPESP (São Paulo state agency, Thematic Project 2013/26258-4). P.A. would like to thank CFisUC for travel support. B.V.C. acknowledges support from the CNPq (Project 306692/2013-9) and from FAPESP (Thematic Project 2017/05660-0).

-
- [1] J. N. Ginocchio, Phys. Rev. Lett. **78**, 436 (1997).
 - [2] J. N. Ginocchio, Phys. Rep. **414**, 165 (2005).
 - [3] J. Meng, K. Sugawara-Tanabe, S. Yamaji, P. Ring, and A. Arima, Phys. Rev. C **58**, R628 (1998).
 - [4] H. Liang, Physica Scripta **91**, 083005 (2016).

- [5] L. N. Savushkin, S. Marcos, M. Lopez-Quelle, and R. Niembro, *Phys. Atom. Nucl.* **69**, 1233 (2006).
- [6] H. Liang, J. Meng, S. G. Zhou, *Phys. Rep.* **570**, 1 (2015).
- [7] P. Alberto, M. Fiolhais, M. Malheiro, A. Delfino, and M. Chiapparini, *Phys. Rev. Lett.* **86**, 5015 (2001).
- [8] P. Alberto, M. Fiolhais, M. Malheiro, A. Delfino, and M. Chiapparini, *Phys. Rev. C* **65**, 034307 (2002).
- [9] J. Meng, K. Sugawara-Tanabe, S. Yamaji, and A. Arima, *Phys. Rev. C* **59**, 154 (1999).
- [10] J. Meng, H. Toki, S. G. Zhou, S. Q. Zhang, W. H. Long, and L. S. Geng, *Prog. Part. Nucl. Phys.* **57**, 470 (2006).
- [11] D. Vretenar, A. Afanasjev, G. Lalazissis, and P. Ring, *Phys. Rep.* **409**, 101 (2005).
- [12] S. S. Zhang, J. Meng, S. G. Zhou, and G. C. Hillhouse, *Phys. Rev. C* **70**, 034308 (2004).
- [13] B.-N. Lu, E.-G. Zhao, and S. G. Zhou, *Phys. Rev. Lett.* **109**, 072501 (2012).
- [14] B. V. Carlson and D. Hirata, *Phys. Rev. C* **62**, 054310 (2000).
- [15] R. Lisboa, M. Malheiro, and B. V. Carlson, *Int. J. Mod. Phys. E* **16**, 3032 (2007).
- [16] P. Bonche, S. Levit, and D. Vautherin, *Nucl. Phys. A* **427**, 278 (1984).
- [17] P. Bonche, S. Levit, and D. Vautherin, *Nucl. Phys. A* **436**, 265 (1985).
- [18] R. Lisboa, M. Malheiro, and B. V. Carlson, *Nucl. Phys. B, Proc. Suppl.* **199**, 345 (2010).
- [19] R. Lisboa, M. Malheiro, and B. V. Carlson, *Phys. Rev. C* **93**, 024321 (2016).
- [20] R. Lisboa, M. Malheiro, and P. Alberto, *Phys. Rev. C* **67**, 054305 (2003).
- [21] J. J. Li, J. Margueron, W. H. Long, and N. Van Giai, *Phys. Rev. C* **92**, 014302 (2015).
- [22] A. Leviatan, *J. Phys.:Conf. Ser.* **267**, 012041 (2011).
- [23] Y. K. Gambhir, P. Ring, and A. Thmet, *Annals of Physics* **198**, 132 (1990).
- [24] G. A. Lalazissis, D. Vretenar, and P. Ring, *Phys. Rev. C* **57**, 2294 (1998).
- [25] D. Vretenar, G. A. Lalazissis, and P. Ring, *Phys. Rev. C* **57**, 3071 (1998).
- [26] G. A. Lalazissis, D. Vretenar, P. Ring, M. Stoitsov, and L. Robledo, *Phys. Rev. C* **60**, 014310 (1999).